IEEE Access
Multidisciplinary | Rapid Review | Open Access Journal

Received October 4, 2019, accepted October 28, 2019, date of publication November 4, 2019, date of current version November 15, 2019.

Digital Object Identifier 10.1109/ACCESS.2019.2951196

Internal Temperature Detections of Contaminated Silicone Rubber under Discharge Conditions Based on Fiber Bragg Gratings

YANPENG HAO, (Member IEEE), YUAN FU, JIE WEI, LIN YANG, (Member IEEE), GUIYUN MAO, ZHENGLIN YANG, AND LICHENG LI

School of Electric Power, South China University of Technology, Guangzhou 510640, China

Corresponding author: Lin Yang (eplyang@scut.edu.cn)

This work was supported by the Smart Grid Joint Fund Key Project between the National Natural Science Foundation of China and State Grid Corporation under Grant U1766220.

ABSTRACT Composite insulators are widely used in power grids at home and abroad. The anti-pollution flashover performance, hydrophobicity and hydrophobic migration, and pollution flashover mechanism of composite insulators have been the focus of international attention. Temperature is one of the important parameters to describe the flashover of composite insulators. In this paper, the internal temperatures of a composite insulation sample were detected based on FBGs (fiber Bragg gratings). The sample was layered and made of one layer of silicone rubber 3 mm in thickness and one layer of epoxy-GFRP (Glass Fiber Reinforced Plastics) similar to 220 kV composite insulators. Three gratings were embedded in the interface of the two layers between long and short electrodes on the surface of the sample. Temperature calibration tests were carried out on the gratings in the sample. Then, discharges tests were done on the sample with embedded FBGs. Internal temperatures as well as leakage currents were measured, and the arcs process of the discharges on the sample was photographed. The test conditions are as follows: the output voltage was increased by approximately 0.5 kV/s; the equivalent salt deposit density (ESDD) was about 0.5 mg/cm^2 and the non-soluble deposit density (NSDD) was about 1.2 mg/cm^2.The results show that the internal FBGs could sense the flashover on the surface of the sample. An interface temperature rise caused by the discharges is within 11 °C in this paper. There is a time delay of 1.4 s from the leakage current arise to the temperature rise during the discharges. The arcs always develops from the small electrode to the large electrode on the surface of the sample, the rise process of the internal temperature at the interface under the middle surface position of the two electrodes is significantly different from that near the small electrode, the arcs starting electrode, while similar to that near the large electrode, the flashover electrode.

INDEX TERMS Fiber Bragg gratings, internal temperature, contaminated silicone rubber, discharges.

I. INTRODUCTION

Composite insulators have the advantages of good anti-pollution performance, small size, light weight, high mechanical strength, less maintenance and convenient transportation, are widely used in power grids at home and abroad [1]. According to statistics, the total length of 110 kV and above overhead lines in China has reached 103 million kilometers by 2019. Meanwhile, the number of composite insulators used in 110 kV and above transmission lines in China has exceeded 10 million by March 2019 [2]. The excellent pollution flashover resistance of composite insulators is a main reason for its wide use. The anti-pollution flashover performance, the hydrophobicity and hydrophobic migration, the pollution flashover mechanism of composite insulators have been the focus of international attention.

In 1958, Obenaus F. proposed the physical model of a local arc and a residual pollution resistance for pollution flashover [3]. Subsequently, surface discharges of contaminated insulation were investigated by domestic and

The associate editor coordinating the review of this manuscript and approving it for publication was Xue Zhou.

foreign scholars. In 2006, Zhang Z. J. summarized the important symptoms in diagnosing the condition of insulators and the relationships between flashover voltage and pollution or atmospheric pressure [4]. In 2008, Zhang Z. J. summarized the pollution flashover mechanism of composite insulators and pointed out that the formation and development of local arc is a key stage for pollution flashover [5].

A plate model is an effective way to study surface discharges of contaminated insulation. Using a plate model in the 1990s, Zhang R. Y. investigated the AC arcs on the surface of a polluted glass. It was found that the length, temperature and brightness of arcs changed periodically with leakage current. The amplitude of current and the length of local arc increased sharply at the moment of flashover, and the core temperature of arcs reached 14000K [6]–[8]. In 2013, Li J. used a triangular glass plate to study the development mechanism of the arc on contaminated surface. It was found that the main reason for arc root movements was the breakdowns at the front end of arc [9]. In 2015, Sun X. F. used a triangular silicone-rubber plate to study the effect of water droplets on the arcs under DC electric field and proposed that the electric field distortion caused by separated droplets was the reason for local arc initiation [10].

Temperature is one of the important parameters to describe flashover of composite insulators. In 2000, Vitelli M. simulated the surface temperature distribution of outdoor contaminated insulators. It was found that the smaller the thickness of a contaminated layer, the lower the probability of a dry zone formation and the lower the peak temperature of the contaminated layer [11]. In 2004, Skopec A. measured the temperature in composite insulation by a thermocouple. The relationship between the internal temperature and the surface temperature was established. Meanwhile, the relationship between the surface temperature under arc discharges and the heat flux density was calculated. The time-domain temperature variations of a composite insulator exposed to arc discharges were studied [12]. In 2014, through infrared thermal imaging technology, Liang F. found that the insulating surface of a rectangular glass plate presented local persistent high temperature before the formation of a dry zone during the process of pollution flashover. After stabilization, the middle temperature in the dry zone was the highest. The temperature symmetrically decreased from the middle of the dry zone to two sides of both electrodes. Furthermore, if the equivalent salt deposit density (ESDD) increased, the formation time of dry zone would shorten and the width of dry zone would decrease [13], [14]. In 2018, Zhang D. experimentally studied the influence of surface resistivity, distributed voltage and wind on the surface temperature distribution of wet contaminated basin insulators. In addition, the heating and discharge mechanism of wet contaminated basin insulators were discussed [15].

The temperature sensing technology by optical fiber has rapidly developed in recent years. In 2013, Luo J. B. established a distributed optical-fiber sensing system with an accuracy of 2 °C to detect the core temperature of overhead lines [16]. Du S. implanted FBGs into the GFRP rod of a composite insulator with a temperature coefficient of 13.5∼14.1 pm/°C [17]. In the same year, the experiments including GFRP fracture, sheaths damage and end fittings crimped degree of the composite insulator with embedded FBGs were carried out by Wen S. to study the relationship between thermal strain and FBG wavelength was studied by the above experiments. It was shown that the temperature sensitivity coefficient of the grating in crimping zone obviously increases with the increase of the lateral pressure of end fitting [18]. In 2017, the internal temperature conversion coefficient of gratings in a composite insulator was studied by Chen and Tang [19].

The purpose of this paper is to study whether the FBGs embedded into composite insulation could detect contaminated flashover on the insulation, what the maximum temperature rise of the FBGs in insulation is, what the time-domain relationship between leakage current and internal temperature rise is, and whether the internal temperatures under short-distance contaminated flashover are different. According to the structure and size of the rod and sheath of 220 kV composite insulators, a two-layer plate sample was made with embedded FBGs. The temperature calibration tests on the FBGs embedded in the sample and the discharge tests of the contaminated sample were carried out in laboratory. The leakage current and internal temperature were measured, and the arc process of discharges was photographed. A method of detecting the internal temperature distribution under surface polluted discharges by FBGs is investigated.

II. DETECTION PRINCIPLE

Fiber Bragg Grating (FBG) is a diffraction grating formed by the periodic axial modulation of the refractive index of the fiber core. In engineering applications, the variation of temperature and strain around the grating will change the cycle of refractive index distribution, and shift the corresponding reflection or transmission wavelength. According to the relationship between wavelength offset and influencing factors, temperature and strain can be calculated.

The peak wavelength of the reflection of the FBG λ_B will change due to the thermal expansion and thermo-optic effect of the FBG when the temperature changes [20], which is expressed as

$$\lambda_B = 2n_{eff} \times \Lambda \tag{1}$$

where n_{eff} is the effective refractive index of FBG, and Λ is the cycle of FBG.

Taking the derivative of temperature T in equation (1), and (1) can be written as

$$\frac{d\lambda_B}{dT} = 2n_{eff} \times \frac{d\Lambda}{dT} + 2\Lambda \times \frac{dn_{eff}}{dT} \tag{2}$$

Combining equation (1) and (2):

$$\frac{d\lambda_B}{\lambda_B} = \left(\frac{1}{\Lambda} \times \frac{d\Lambda}{dT} + \frac{1}{n_{eff}} \times \frac{dn_{eff}}{dT}\right) \times dT \tag{3}$$

If letting $\zeta = \frac{1}{n_{eff}} \times \frac{dn_{eff}}{dT}$, $\alpha = \frac{1}{\Lambda} \times \frac{d\Lambda}{dT}$, then

$$\frac{d\lambda_B}{\lambda_B} = (\alpha + \zeta) \times dT = K_T \times dT \quad (4)$$

$$\Delta\lambda_B = K_T \times dT \quad (5)$$

where α is the thermal expansion coefficient, ζ is the thermo-optical coefficient, K_T is the temperature coefficient related to central wavelength offset, ΔT is the temperature variation and $\Delta\lambda_B$ is the wavelength offset.

The change of reflective wavelength of FBG is also affected by strain. In sensing applications, special encapsulation can make gratings unaffected by strain to make temperature sensors.

III. EXPERIMENTS

A. TEST SYSTEM

The test system includes filter, voltage regulator, transformer, test product and computer, as well as discharge video camera unit, FBG demodulator and leakage current measurement device, as shown in Fig. 1.

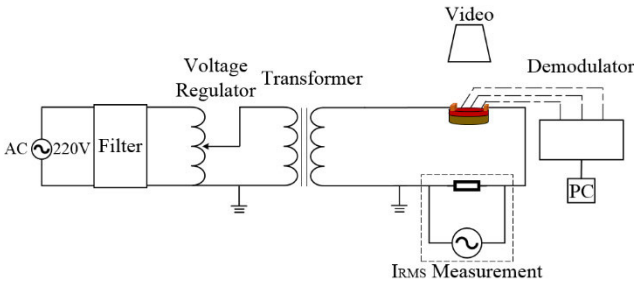

FIGURE 1. Schematic diagram of test and measurement equipment.

A 220 V, 50 Hz power source was connected to the voltage regulator with 1.5-500 kVA capacity through a 200 V/30 A, 6 kVA low-pass filter with non-partial discharge. A 50 kV/120 mA, 6 kVA transformer was a light pneumatic non-partial discharge test transformer which its partial discharge was less than 5 Pc.

The implanted FBG parameters of test sample are shown in Table 1. A demodulator with JEME-iFBG0-S08, 1510-1590 nm wavelength, 1 pm accuracy, 10 Hz scanning frequency recorded the wavelength data during the experiment. The FBGs were connected to the demodulator by optical fiber.

TABLE 1. Parameters of FBGs.

Parameters	FBG2	FBG2	FBG3
Wavelength/mm	1544.359	1526.769	1557.976
Reflectivity/%	93.51	91.88	92.55
Bandwidth/nm	0.183	0.192	0.197
SMSR/dB	15.75	16.0	16.5
Grating length/mm	10	10	10

Leakage current was recorded twice per second by UT61E RMS module.

The arc process camera was Canon EOS 5D MARK II with 1920 × 1080 image resolution and 30 fps.

B. TEST SAMPLE

The types and structural parameters of composite suspension insulators commonly used in transmission lines are shown in Table 3. It is evident that the GFRP rod's diameter and housing's thickness of 10 kV, 110 kV and 220 kV composite suspension insulators are 18 mm and 4 mm respectively. In this paper, silicone rubber-epoxy-GFRP double-layer plate sample are made with the same material as composite suspension insulators in service. The parameters are shown in Table 2.

TABLE 2. Parameters of the sample.

Sample	Shape	Volume[mm]
Silicone rubber	circle	$\pi 50^2 \times 4$
Epoxy-GFRP	circle	$\pi 50^2 \times 9$

TABLE 3. Structure parameters of composite suspension insulators.

Type	RD	HT	BSD	SSD
FXBW-10/70	18	4	122	74
FXBW-110/120	18	4	122	74
FXBW-220/120	18	4	122	74
FXBW-500/120	28	5.5	142	98
FXBW-1000/210	28	6	175	131

RD = Rod's diameter [mm], HT=Housing thickness [mm], BSD=Big sheds diameter [mm], SSD=small sheds diameter [mm].

Two copper electrodes, long and short, were arranged in parallel on the surface of silicone rubber plate with sizes of 70 × 10 × 10 mm^3 and 20 × 10 × 10 mm^3, respectively. The distance between the two electrodes was about 75 mm. On the other surface of the silicone rubber plate, there were three elongated grooves equally spaced at the distance between the two electrodes. The groove depth and width were both 1 mm, and the distance from the short electrode were 10 mm, 42.5 mm and 75 mm, respectively. Diagram are shown in Figs. 2(a). FBGs were placed in the groove and filled with Room Temperature Vulcanized Silicone Rubber (RTV). After above RTV solidified, the grooved side surface of silicone rubber was bonded with epoxy GFRP circular plate by RTV again, and then a silicone rubber-epoxy-GFRP circular plate sample embedded with three grating sensors was fabricated, as shown in Figs. 2(b). The positions of FBG1, FBG2 and FBG3 were located on the central line of the two electrodes, as shown in the red part of Figs. 2(c). In this paper, the FBG was not encapsulated and directly contacted with silicone rubber and RTV.

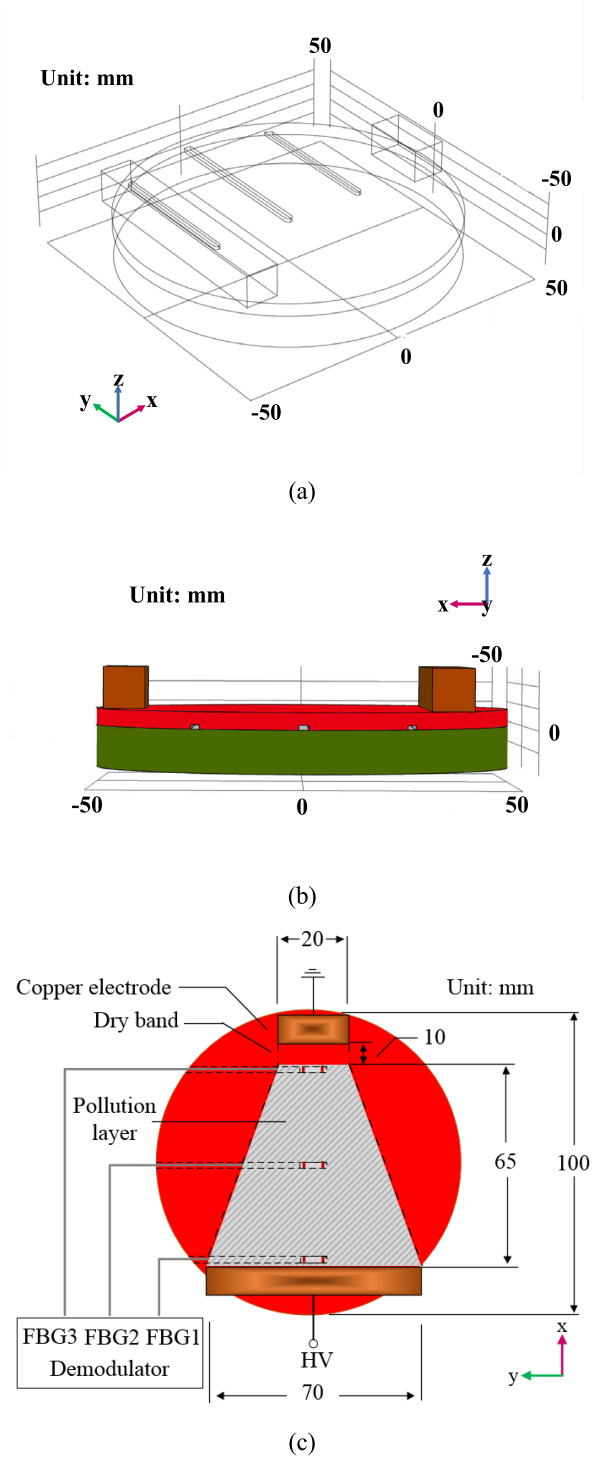

FIGURE 2. Plate model of silicone rubber-epoxy-GFRP samples. (a) Perspective view, (b) lateral view, (c) schematic diagram of FBG and surface contamination zone.

C. TEMPERATURE CALIBRATION TEST

Temperature calibration test was carried out on grating temperature sensor implanted in the sample. The test was completed in a constant temperature and humidity box, model HSP-250BE. The surface temperature of the sample is equal to the temperature in the box. The internal temperature at the grating is the same as that at the surface after several hours. Therefore, the relationship between the grating wavelength and the temperature at the grating can be calibrated. The process was as follows:

1) The silicone rubber-epoxy-GFRP round plate sample embedded with FBGs was put into the constant temperature and humidity box. The optical fiber was pulled out from the box, and connected with the demodulator and computer. The scanning time of the demodulator was 100 ms.

2) The temperature of the box was regulated to 13 °C, 26 °C, 32 °C, 38 °C, 46 °C, 52 °C, 55 °C and 59 °C, respectively, and the humidity was 65 %. The grating wavelength of the sample was continuously recorded until the wavelength variation value was stable (< 10 pm/min). It takes about 8 hours for composite suspension insulator to reach the same temperature inside and outside [17]. In the accordance of above time, it will take several hours for the internal and external temperatures of the sample to be uniform. In the whole process described here, the sample must be kept static in the box.

D. POLLUTION DISCHARGE TEST

As mentioned above, the contaminated area on the surface of the sample was a trapezoid to reduce the change of arc position as far as possible. The two electrodes at both edges of the trapezoid were copper blocks with different lengths stated in Section III *B*. The 10 mm wide dry-band was set aside near the short edge of electrodes in the polluted area for simulating the dry-band of pollution discharge of composite insulator in service. Therefore, the practical length of polluted area was about 65 mm, as shown in Figs. 2(c).

In the accordance of standard [21], the sample needs to be cleaned with tap water and ethyl alcohol before being polluted. After drying, a layer of dry kaolin was uniformly coated on the surface of the sample with a soft brush. Quantitative brushing method was used to contaminate the sample. The contamination solution consisted of kaolin, NaCl and deionized water. The ratio of NaCl and kaolin was 1:2.4. The equivalent salt deposit density (ESDD) was 0.5 mg/cm^2 and the non-soluble deposit density (NSDD) was 1.2 mg/cm^2. The process was as follows:

1) The silicone rubber surface was contaminated.

2) The voltage was directly applied to the sample when it was moist. At the beginning moments of voltage variation, the video, FBG demodulator and leakage current measurement were started at the same time. In this paper, the uniform boosting method was adopted [22].

3) The voltage was boosted evenly to 10 kV in 20 seconds. After the achievement of 10 kV, the voltage was maintained for 60 seconds.

IV. RESULTS AND DISCUSSION

A. THE RELATIONSHIP BETWEEN GRATING WAVELENGTH AND TEMPERATURE

The experimental results of grating temperature calibration in the HSP-250BE are shown in Fig. 3. Fig. 3 shows that the wavelength of the grating is linear with temperature.

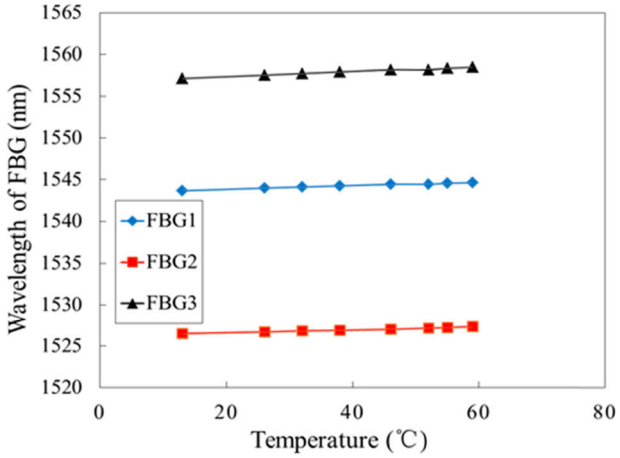

FIGURE 3. Relationship between the wavelength of FBGs and the temperature inside the sample.

The goodness of fit R^2 all are approximately 0.99. The gradients of three straight lines in the Fig. 3 are temperature sensitivity. The temperature sensitivity of FBG1, FBG2 and FBG3 are 20.4 pm/°C, 17.2 pm/°C and 28.8 pm/°C, respectively.

The temperature sensitivity of bare FBG is generally about 13.2 pm/°C. In addition, the temperature sensitivity is related to the effective index, thermo-optical coefficient and thermal expansion coefficient of FBG. Therefore, the FBGs embedded with the sample was affected by the contact material so that the temperature sensitivity was high. The difference of temperature sensitivity of the three gratings may be due to the incomplete uniformity of manual implantation, which results in different thermal expansion of materials in the FBG's area. However, the accuracy of temperature calibration test is still precise.

B. LOCAL ARCS CHARACTERISTICS

The surface discharges of insulators have large randomicity [23]. According to the severity of surface discharges, the surface discharges of insulators can be divided into three types: weak discharges, intermittent arc discharges and continuous arc discharges.

Weak discharges: Corona discharges or filamentary discharges are generated on the insulating surface, which is characterized by sporadic sparks and small arcs. The range of sparks or arcs on the surface is small. Furthermore, the duration of sparks or arcs is extremely short, which is characterized by sudden appearance and instantaneous disappearance (See Figs. 4(a)).

Intermittent arc discharges: More intense arcs are produced on the insulating surface. The arc range is larger, but the duration is relatively short, as shown in Figs. 4(b).

Continuous arc discharges: Severe arcs are produced repeatedly on the insulating surface. The arc range is extremely large, and the duration is long. As shown in Figs. 4(c), arcs almost bridge two electrodes and sometimes arcs may levitate from the surface.

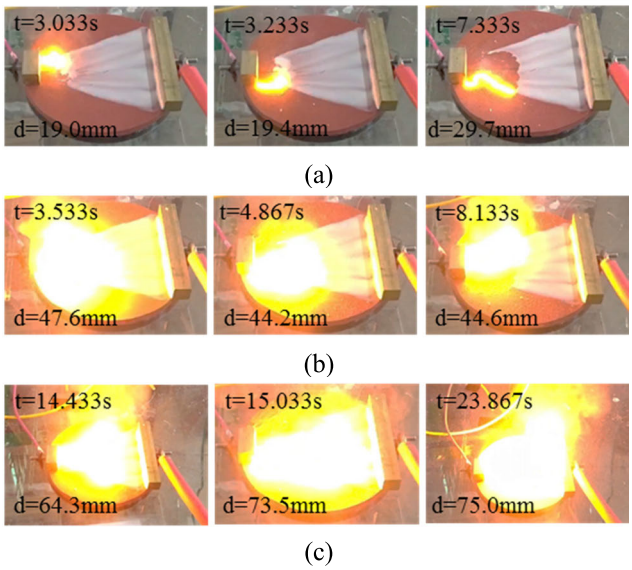

FIGURE 4. Typical surface discharges on contaminated insulation. (a) Weak discharges, (b) intermittent arc discharges, (c) continuous arc discharges.

TABLE 4. Duration and arc length of discharges on contaminated surface.

Content	Weak discharges	Intermittent arc discharges	Continuous arc discharges
t_d/ms	<67	<167	>167
d/mm	<42.5	<57.5	<75

Fig. 4 shows the appearance moment t_d and the length d of arcs, where d is the vertical distance between the initial electrode and the farthest point of arc propagation. Through numerous tests, the duration and arc length of various types of discharge are shown in Table 4.

C. LEAKAGE CURRENT

In the differences of above three discharges types, the leakage current is also an important parameter besides the duration and arc length. The leakage current I_{rms} in the discharges process is shown in Fig. 5.

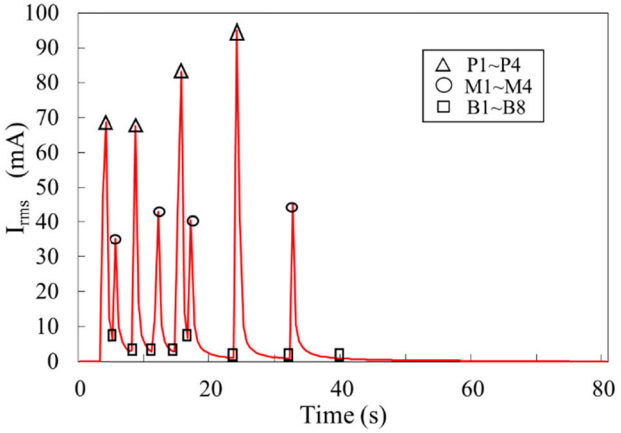

FIGURE 5. Leakage current I_{rms} of discharges process on contaminated surface. (0.5 kV/s, ESDD was 0.5 mg/cm^2 and NSDD was 1.2 mg/cm^2).

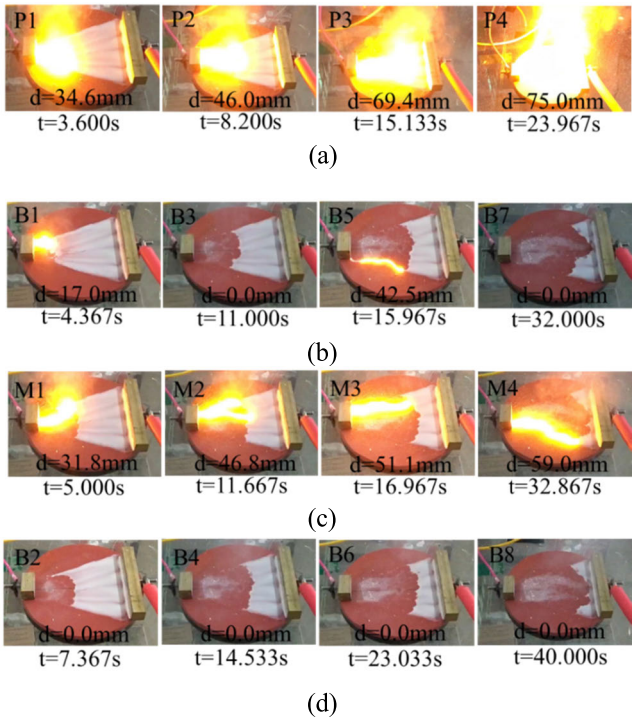

FIGURE 6. Image of discharges process on contaminated insulated surface. (a) P1-P4, (b) B1, B3, B5, B7, (c) M1-M4, (d) B2, B4, B6, B8.

Fig. 5 shows that large and small current pulse occurred at intervals. In chronological order, P1∼P4 are the peak points of large pulses; M1∼M8 are the peak points of small pulses; B1∼B8 are the trough points of current. The discharges images of corresponding time are shown in Figs. 6.

From Fig. 5, it can be seen that the occurring of arc concentrated in 3 s∼17 s. The time intervals of M3, P4 and M4 are about 7 s and 6 s respectively, whereas those of M1, P2 and M2 are about 3 s and 4 s respectively. It can be found that the leakage current is the largest when the two electrodes are connected by arcs. Meanwhile, the time interval of M3, P4 and M4 is about twice as long as the time interval of the existence of the local arc.

From Fig. 5 and Figs. 6, there was no arc on the contaminated insulating surface when the time was from 0∼2.5 s and 40∼80 s. Furthermore, the leakage current was 0 mA within periods of above time. In the points of P1-P4, the leakage current was large; the arcs on the insulating surface were intense; the length of arcs was long and the discharges area was large. In the points of M1-M8, the leakage current was small; the arcs were intense; the arc length was large and the discharges area was small; in the points of B1-B8, the leakage current was extremely small, and there may be arc with small length and area, or even no arc occurs.

In addition, a sudden increase in leakage current represents that arcs exist on the insulating surface. The discharges are intermittent when the current reaches about 67 mA; the discharges are continuous when the current reaches 83 mA; the arcs levitate from the surface when the current reaches 95 mA.

In summary, the time of arc appearance on contaminated insulating surface is consistent with the peak points of leakage current. The leakage current (RMS) can be used to characterize the severity of discharge.

According to the time evolution from the top to bottom of the left column to the top to bottom of the right column (see Figs. 6), it can be seen that the surface arcs presented the phenomenon of repeated starting and extinguishing. The arcs may levitate from the surface due to thermal buoyancy, as shown in the images of P3 and P4 (Figs. 6(a)).

D. COMPREHENSIVE ANALYSIS OF INTERFACE TEMPERATURE AND LEAKAGE CURRENT

The internal temperature of surface contamination discharges is obtained through wavelength-temperature calibration relationship, as shown in Fig. 7. It should be mentioned here that the relative ambient temperature is 20.5 °C. Also, the lengths d of arcs corresponding to the current pulse time are shown in Fig. 7.

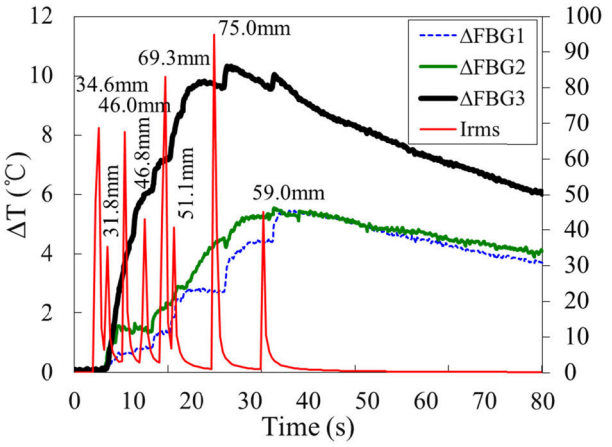

FIGURE 7. Time evolution of temperature rise, arcs length and leakage current during discharges on contaminated insulation surface.

From Fig. 7, it can be seen that one current pulse corresponds to one temperature rise. Then, the temperature decreases slowly after the pulse. Therefore, the temperature curve has obvious steps of rise, saturation or slow drop when there are several leakage current pulses in the process of pollution discharge.

In this paper, three characteristic parameters, the starting time of temperature rise t_1, the variation of temperature rise ΔT and the time reached peak temperature t_m, are proposed to characterize the trend of internal interface temperature of the sample during surface contamination discharges.

The starting time of temperature rise t_1: If the temperature of five consecutive times are higher than the initial temperature T_0 from the boost of voltage and the trend is increasing, then the first time of the five times will be the starting time of temperature rise t_1.

The variation of temperature rise ΔT and the time reached peak temperature t_m: The variation of temperature rise ΔT equals the maximum temperature subtract the T_0. The time

reached peak temperature t_m should satisfy the condition that the temperature in $t_m \pm 5$ is less than the maximum temperature within that time period.

Variation characteristics of temperature measured by FBGs embedded in the sample are shown in Table 5. The λ_0 is the initial center wavelength.

TABLE 5. Variation characteristics of wavelength and temperature of FBGs embedded in the sample.

Variables	FBG1	FBG2	FBG3
t_1/s	5.4	5.3	5.4
t_m/s	37.7	34.1	26.1
λ_0/nm	1543.808	1526.569	1557.415
T_0/°C	20.5	20.5	20.5
ΔT/°C	5.5	5.5	10.3

First of all, it can be seen from Table 5 that the t_1 of three FBGs are almost identical. The heat can also be transmitted to different internal positions with a thickness of 3 mm and a distance of 65 mm at the same time, even if the weak discharges occur. Secondly, as shown in Fig. 6 and Fig. 5, the starting time of temperature rise t_1 of the three FBGs are about 5.4 s, which lagged 1.4 s behind the moment of sudden increase of leakage current ($t = 4$ s). This is because of the time of heat transfer from the surface to the interface. Moreover, the thermal conductivity of silicone rubber material is about 0.6 J/m·k. The FBGs are located at the depth of about 3 mm from the polluted discharge surface so that a certain time that the heat of the discharge surface transferring to the interface is needed.

Also, it can be seen that the ΔT of FBG1 and FBG2 are the same as 5.5 °C, which are obviously less than 10.3 °C of FBG3. The ΔT of FBG3 is relatively high because it is located near the accessory of arcing electrode. As shown in Fig. 7, the arc length of first peak is 34.6 mm, which reaches the corresponding insulating surface position of FBG2, but not to FBG1. Then, except for the arc of second peak, each arc reached the position near FBG1. However, the ΔT of FBG2 is almost the same as that of FBG1. This reflects that the effect of arc heat transfer from surface to interface on interface temperature may be equivalent to that of leakage current without arc. The time evolution of the variation of temperature rise between FBG2 and FBG1 is not entirely consistent, and t_m is also slightly different, but there is still a significant difference between FBG3 and FBG2 (or FBG1).

ΔT is mainly affected by convective heat dissipation and conductive heat dissipation. Most of the heat loss is due to convective heat dissipation with air during the transfer of arc heat to the insulating surface; part of the heat loss is due to conductive heat dissipation during the transmission of temperature from the insulating surface to the interior of the insulation. Therefore, the arc with a temperature of up to 1000 degrees in a short time caused only several degrees of temperature variation in the insulation interior.

V. CONCLUSION

According to the material and the size of composite suspension insulator, a silicone rubber-epoxy GFRP circular plate sample embedded with three FBGs temperature sensors were fabricated. The interface temperature between silicone rubber and epoxy-GFRP were detected by FBG. Combining with the characteristics of local arc and leakage current analysis, this paper studies the process of contaminated discharge by measuring temperature with internal FBG. The conclusions are as follows:

1) The temperature sensing of contaminated discharge on the surface of silicone rubber is realized by the FBG of 3 mm thick interface between silicone rubber and epoxy-GFRP. The FBG implanted on the interface provides an effective detection technology for the study of the discharge process on the contaminated insulating surface.
2) The leakage current increases sharply due to the arc generated on the polluted insulating surface. The temperature rises at the inner interface of 3 mm insulation after a certain delay of about 1.4 s. The leakage current is consistent with the discharge intensity in time domain. The interface temperature does not rise when there is no leakage current on the contaminated insulating surface.
3) If the arc always starts at one end of the electrode and develops to the other electrode during the discharge on the contaminated insulation surface with short gap, the internal temperature near the arc starting electrode differs greatly from the temperature at the middle position of the two electrodes, while the temperature at the middle position differs little from that near the flashover electrode.

With the help of FBG temperature sensor implanted in composite insulation, the further study will be: the effectiveness of FBG temperature sensor in thicker (such as UHV) sheaths: the relationship between temperature distribution and leakage current in the process of wetting-drying of insulating surface: the relationship between the characteristics of starting and developing of contaminated local arc, temperature distribution and leakage current; the critical conditions for the development of local arc on polluted insulation surface to final flashover. Through these studies, the discharge process and mechanism of contaminated surface can be improved.

REFERENCES

[1] M. Lu, *Composite Insulator Technology and Fault Case Analysis*. 1st ed. China: Elect. Power Press, 2018, pp. 22–65.

[2] Z. Zhang, "Study on high temperature degradation characteristics and interface detection of high voltage side of composite insulator," Ph.D. dissertation, Dept. Elect. Eng., Tsinghua Univ., Beijing, China, 2019.

[3] F. Obenaus, "Fremdschichtueberschlag und Kriechweglaenge," *Deutsche Elektrotechnik*, vol. 12, no. 4, pp. 135–136, 1958.

[4] Z.-J. Zhang, X.-L. Jiang, and C.-X. Sun, "Present situation and prospect of research on flashover characteristics of polluted insulators," *Power Syst. Technol.*, vol. 30, no. 2, pp. 35–40, Jan. 2006.

[5] Z. Zhang, X. Jiang, and C. Sun, "Summary of research on flashover mechanism of polluted insulators," *Power Syst. Technol.*, vol. 32, no. 16, pp. 37–42, Aug. 2008.
[6] S. Li, R. Zhang, and K. Tan, "The study of electric arc propagating along a polluted dielectric surface under AC voltage," *Proc. CSEE*, vol. 11, no. 2, pp. 1–7, Mar. 1991.
[7] R. Zhang, Z. Guan, J. Xue, D. Zhu, and K. Tan, "The study of discharge along a polluted dielectric surface," *Prog. Natural Sci.*, vol. 6, no. 1, pp. 39–47, Jan. 1996.
[8] S. Li, R. Zhang, and K. Tan, "The mechanism of pollution flashover," *J. Tsinghua Univ.*, vol. 31, no. 1, pp. 7–15, Jan. 1991.
[9] J. Li, "Study of the mechanism of arc propagation over a polluted insulation surface and the time-varying model," Ph.D. dissertation, Dept. Elect. Eng., Tsinghua Univ., Beijing, China, 2013.
[10] X. Sun, "Study on DC arc characteristics and its influence factors on silicone rubber surface," M.S. thesis, Dept. Elect. Eng. Chongqing Univ., Chongqing, China, 2015.
[11] M. Vitelli, V. Tucci, and C. Petrarca, "Temperature distribution along an outdoor insulator subjected to different pollution levels," *IEEE Trans. Dielectrics Electr. Insul.*, vol. 7, no. 3, pp. 416–423, Jun. 2000.
[12] A. Skopec, L. Moron, and P. Zylka, "Time-domain temperature variations of a composite insulator surface exposed to arc discharges," *IEEE Trans. Dielectrics Electr. Insul.*, vol. 11, no. 2, pp. 369–377, Apr. 2004.
[13] F. Liang, M. Macalpine, and Z. Guan, "Formation of dry-band in the process of pollution flashover based on infrared thermal image analysis," *High Voltage Eng.*, vol. 40, no. 1, pp. 138–146, Jan. 2014.
[14] F. Liang, M. Macalpine, and Z. Guan, "Factors affecting dry- band formation on the surface of polluted insulator," *High Voltage Eng.*, vol. 38, no. 10, pp. 2604–2610, Oct. 2012.
[15] D. Zhang, "Heating and discharge mechanism of wet contaminated insulators," *High Voltage Eng.*, vol. 44, no. 3, pp. 787–795, Mar. 2018.
[16] J. Luo, Y. Hao, Q. Ye, Y. Hao, and L. Li, "Development of optical fiber sensors based on Brillouin scattering and FBG for on-line monitoring in overhead transmission lines," *J. Lightw. Technol.*, vol. 31, no. 10, pp. 1559–1565, May 15, 2013.
[17] S. Du, W. Cai, and H. Deng, "Production and calibration test of the composite insulator with fiber Bragg grating embedded," *High Voltage Eng.*, vol. 38, no. 10, pp. 2774–2780, Oct. 2012.
[18] S. Wen, W. Cai, H. Deng, S. Du, R. Ke, and P. Xiong, "Fault simulation experiment on composite insulators with fiber Bragg grating implanted," *High Voltage Eng.*, vol. 39, no. 1, pp. 81–87, Jan. 2013.
[19] W. Chen and M. Tang, "Monitoring on internal temperature of composite insulator with embedding fiber Bragg grating for early diagnosis," in *Proc. 25th Opt. Fiber Sensors Conf.*, Jeju, South Korea, Apr. 2017, pp. 1–4.
[20] X. Qiao, Z. Jia, and H. Fu, "Theory and experiment about in-fiber Bragg grating temperature sensing," *Acta Phys. Sinica*, vol. 53, no. 2, pp. 494–497, Feb. 2004.
[21] *Artificial Pollution Tests on Composite Insulators Used on High-Voltage AC Systems*, document DLT 859-2015, 2015.
[22] C. Zhang, F. Zhang, and R. Li, "Comparison of on-load voltage methods in artificial contamination test for insulators," *High Voltage Eng.*, vol. 39, no. 1, pp. 44–53, 2013.
[23] Q. Zhang, J. Zhou, and H. Xi, "Discharge features of composite insulator in different surface states," *High Voltage Eng.*, vol. 40, no. 4, pp. 987–994, Apr. 2014.

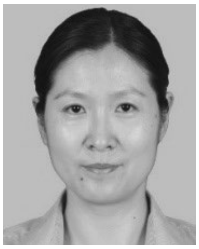

YANPENG HAO (M'13) was born in Hebei, China, in 1974. She received the B.S. and Ph.D. degrees in electrical engineering from Xi'an Jiaotong University, China, in 1998 and 2003, respectively. She was a Postdoctoral Researcher with Tsinghua University, from 2003 to 2005. She is currently a Professor with the South China University of Technology (SCUT), Guangzhou, China. Her main research interests include insulation condition monitoring and operation safety of electric power equipment, and dielectric barrier discharge under atmospheric pressure.

She is the Leader of the High Voltage Group, SCUT. She is also a Commissioner of the Professional Committee on High Voltage of the Chinese Society for Electrical Engineering, a member of the Professional Committee on Engineering Dielectric of the China Electrotechnical Society, and the Executive Chairman of the 2nd IEEE International Conference on Electrical Materials and Power Equipment (ICEMPE 2019).

YUAN FU was born in Guangxi, China, in 1994. He received the B.S. degree in electrical engineering and automation from the Chengdu University of Technology, China, in 2017. He is currently pursuing the M.S. degree with the South China University of Technology, Guangzhou, China. His main research interest includes temperature characteristics of composite insulator under pollution discharge.

JIE WEI was born in Guangxi, China, in 1992. He received the B.S. degree in electrical engineering from Chongqing University, Chongqing, China, in 2016. He is currently pursuing the Ph.D. degree in high-voltage engineering with the School of Electric Power, South China University of Technology. His research interests include high-voltage external insulation and online monitoring icing condition of insulators.

LIN YANG (M'13) was born in Hunan, China, in 1984. He received the B.Sc. degree from Guangxi University, Guangxi, China, in 2007, and the Ph.D. degree from the South China University of Technology, Guangzhou, China, in 2012.

He is currently an Associate Professor with the South China University of Technology. His research interests include HV outdoor insulation and overhead transmission lines' online monitoring technology.

GUIYUN MAO was born in Shandong, China, in 1993. He received the B.S. degree in electrical engineering and automation from the China University of Mining and Technology, China, in 2016. He is currently pursuing the M.S. degree with the South China University of Technology, Guangzhou, China. His main research interest includes external insulation characteristics of composite insulators.

ZHENGLIN YANG was born in Shandong, China, in 1995. He received the B.S. degree in electrical engineering from Shandong Agricultural University, China, in 2017. He is currently pursuing the master's degree with the South China University of Technology, Guangzhou, China. His main research interests include external insulation and online monitoring of transmission and transformation equipment.

LICHENG LI was born in Jiangsu, China, in 1941. He received the B.S. degree from the Department of Electrical Engineering, Tsinghua University, Beijing, China, in 1967. He was the Director of the first ±800-kV transmission line project in the world. He also participated in the development of the first 330- and 500-kV ac transmission lines and the first ±500-kV dc transmission lines in China. He is currently an Academician in the Chinese Academy of Engineering, and a Professor and a Doctoral Supervisor with the South China University of Technology. He is also the Secretary of the Expert Committee of the China Southern Power Grid.